Inorganic Chemistry

Article

pubs.acs.org/IC

Density Functional Theory Study of Rh(III)-Catalyzed C−H Activations and Intermolecular Annulations between Benzamide Derivatives and Allenes

Zhong Xing, Fang Huang,* Chuanzhi Sun, Xue Zhao, Jianbiao Liu, and Dezhan Chen*

College of Chemistry, Chemical Engineering and Materials Science, Collaborative Innovation Center of Functionalized Probes for Chemical Imaging in Universities of Shandong, Key Laboratory of Molecular and Nano Probes, Ministry of Education, Shandong Provincial Key Laboratory of Clean Production of Fine Chemicals, Shandong Normal University, Jinan 250014, People's Republic of China

Supporting Information

ABSTRACT: Density functional theory has been applied to gain insight into the Cp*Rh(OAc)$_2$-catalyzed C−H activation and intermolecular annulation of benzamide derivatives with allenes. The study shows that the reactions proceed in three steps: (1) C−H activation induced by Rh catalyst reacting with benzamide derivatives, (2) carborhodation of allene, and (3) regeneration of Rh catalyst. The results indicate that the N−H deprotonation makes the following C−H activation much easier. The regio- and stereoselectivities of **1a** (*N*-pivaloyloxy benzamide)/**2a** (cyclohexylallene) and **1b** (*N*-pivaloyloxy-4-methyl-benzamide)/**2b** (1,1-dimethyl allene) depend on the allene carborhodation step. The steric hindrance effect is the dominant factor. We also discuss the reaction mechanism of **1c** (*N*-methoxy benzamide)/**2a**. The chemoselectivity between **1c**/**2a** is determined by the N−O cleavage step. Replacement of OPiv by OMe leads to loss of the stabilization effect provided by C═O in OPiv. Additionally, Cp*Rh(OAc)(OPiv) is produced in the Cp*Rh(OAc)$_2$ regeneration step, which can work as catalyst as well.

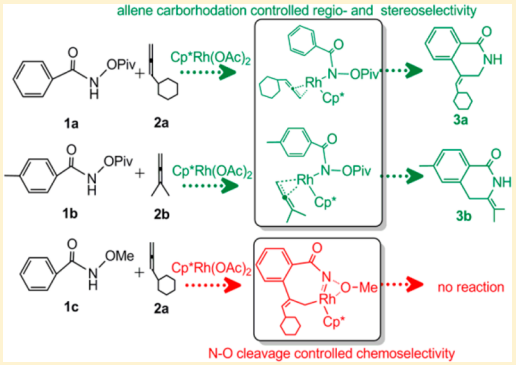

1. INTRODUCTION

The carbometalation reaction of allenes has attracted increasing attention for its highly versatile and reactive π-allyl metal species. Metal-catalyzed cycloadditions have revolutionized the way of making cyclic compounds.[1] Through formal $(3 + 2)^2$ or $(4 + 2)^3$ cycloadditions, a variety of heterocycles are easily constructed. In the seminal work of Larock[4] and the later works of Murakami and Matsubara,[5] several types of halogenated compounds, triazoles, and phthalimides have been used as the starting materials for the synthesis of a variety of heterocycles which can avoid the drawbacks of high temperature, strongly acidic, or basic conditions. However, the experiments of halogenated compounds are complex, and the precursors of triazoles and phthalimides are limited. Thus, straightforward synthesis of heterocycles via C−H activation has attracted much attention. For the past decades, people have devoted much effort to conversion of inactivated C−H bond to C−C or C−N bond.[6,7]

Recently, Wang and Glorius reported the first Rh(III)-catalyzed C−H functionalization reactions with allenes proceeding under mild conditions (Scheme 1).[8] Under the catalysis of $(RhCp^*Cl_2)_2$ and CsOAc in MeOH, 3,4-dihydroisoquinolin-1(2*H*)-ones **3a** (*Z* configuration) is selectively generated from *N*-pivaloyloxy benzamides **1a** and cyclohexylallene **2a** without detection of the isomers **3a**′ and **3a**″, indicating a high regio- and stereoselectivity. On changing **1a** to **1b** and **2a** to **2b**, only isomer **3b** is afforded. However, when changing **1a** to **1c**, no product is observed in experiment. All these phenomena greatly attract us: (1) what are the mechanisms of the reactions? (2) How are the regio- and stereoselectivity controlled by the catalyst for the reactions between **1a** and **2a** and **1b** and **2b**? (3) Why could **1c** and **2a** not react with each other even with the catalyst? In order to answer the above questions and understand the intrinsic mechanism of this experiment, a DFT study was conducted by us. It would give us a better understanding of the chemo-, regio-, and stereoselectivity of the annulations between benzamide derivatives and allenes. Meanwhile, we hope the deep understanding of the mechanism would provide useful information to design high-selectivity catalysts.

2. COMPUTATIONAL DETAILS

All calculations were carried out using the Gaussian 09 suite of computational programs.[9] The hybrid density functional B3LYP[10,11] was employed. Geometries were optimized using the 6-31G(d, p)[12] basis sets on nonmetal atoms and LANL2DZ[13,14] effective core potentials on Rh. Vibrational frequencies were computed at the same level to get the thermal and entropic corrections and to confirm whether the structures are minima or transition states. When necessary, IRC calculations were performed to verify the right connections among a transition state and its forward and reverse minima.[15] Because the M06 functional[16] includes noncovalent interactions and can give accurate energies for transition metal systems,[17] single-point calculations with

Received: January 20, 2015
Published: April 9, 2015

DOI: 10.1021/acs.inorgchem.5b00134
Inorg. Chem. 2015, 54, 3958−3969

Scheme 1. Rh(III)-Mediated Annulations of Benzamide Derivatives and Allenes Reported by Glorius

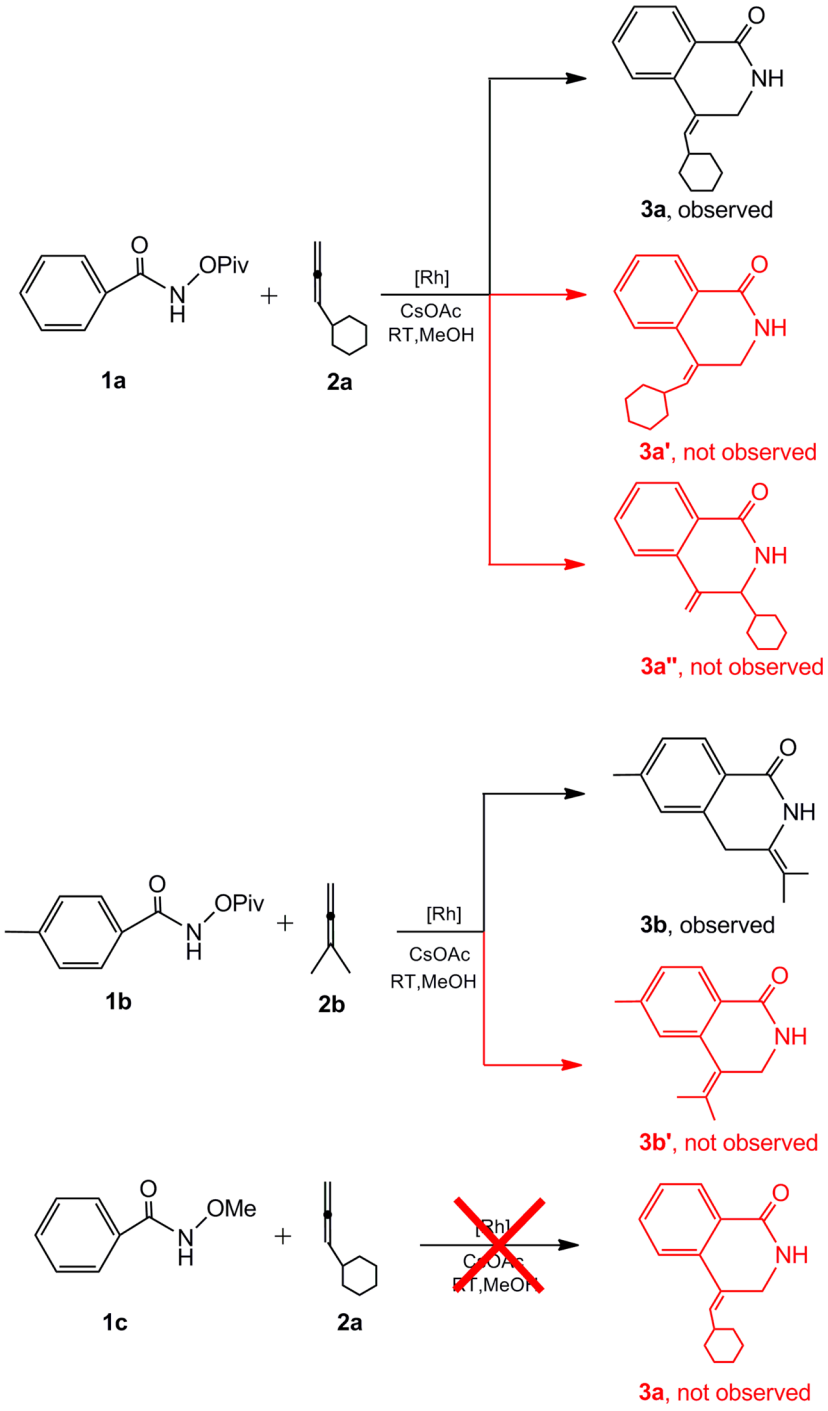

solvation effects modeled by SMD[18] in methanol solvent were applied for all gas-phase-optimized structures at the M06/[6-311++G(d, p)+LANL2DZ] level. The effectiveness of B3LYP for geometry optimizations and M06 for single-point energy calculations has been demonstrated by numerous studies to successfully produce energy profiles of reactions involving transition metal complexes.[19,20] The free energies are used in the following discussion. All optimized structures, as well as their Cartesian coordinates, are given in the Supporting Information.

3. RESULTS AND DISCUSSION

On the basis of the detected products, we discuss our computational results as follows: in sections 3.1−3.4, the detailed mechanism between **1a** and **2a** is described; then the regioselectivity between **1b** and **2b** is illuminated in section 3.5; finally, reaction between **1c** and **2a** is discussed.

3.1. C−H Activation. $Cp^*Rh(OAc)_2$, which is generated by the reaction between $[Cp^*RhCl_2]_2$ and CsOAc, is chosen as the active catalyst in our work, based on the experimental[8,21] and theoretical[22,23] reports. Two pathways (denoted as Path A and Path B) are designed and calculated in this process. In Path A, C−H activation occurs first and is followed by N−H deprotonation. While in Path B, the sequence is inverted to understand the origin of C−H activation. Free energy profiles of the two paths are illustrated in

DOI: 10.1021/acs.inorgchem.5b00134
Inorg. Chem. 2015, 54, 3958−3969

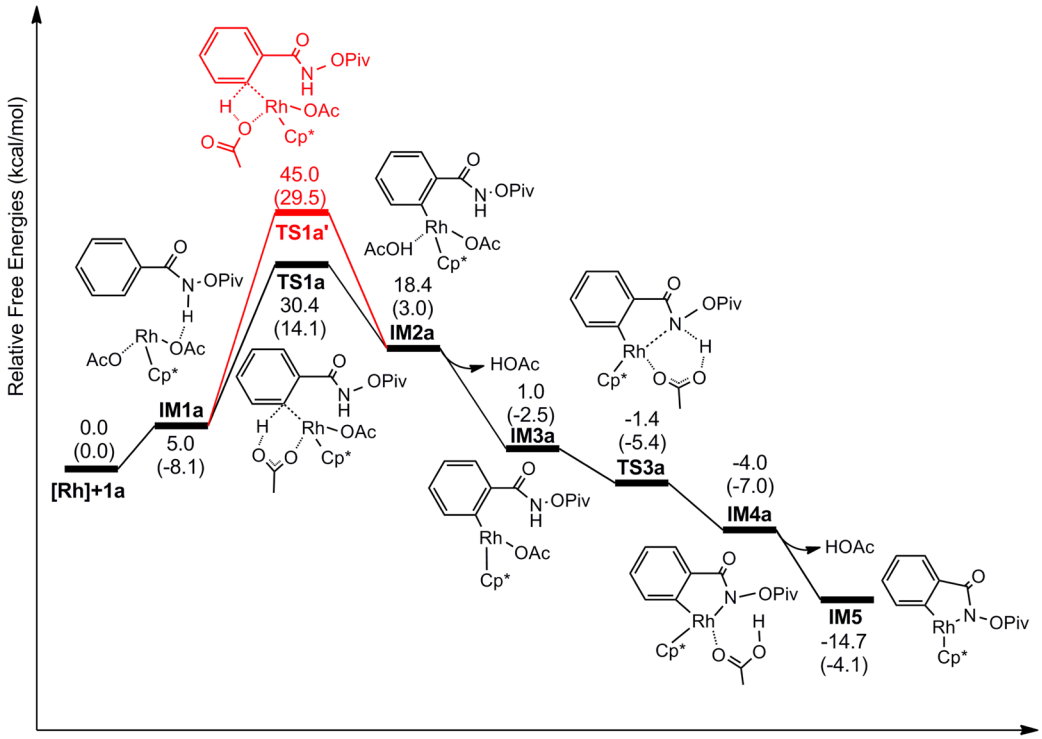

Figure 1. Free energy profile of Path A in the C−H activation step (values are given in kcal/mol; enthalpies are listed in parentheses).

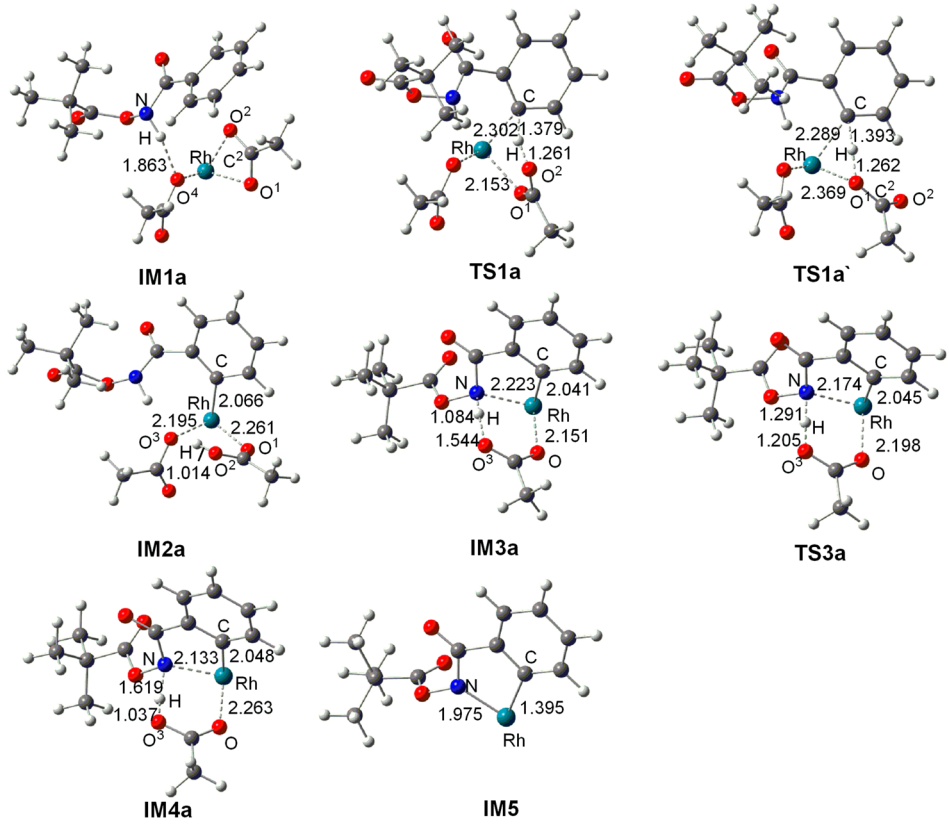

Figure 2. Optimized structures of the stationary points of Path A in the C−H activation step, along with the key bond lengths (in Angstroms). Cp* has been omitted for clarity.

Figures 1 and 3. The key optimized geometries are given in Figures 2 and 4.

In Path A, intermediate **IM1a** is first formed via the hydrogen bond interaction between N−H···O^4 (see Figure 2). The interaction is favorable by 8.1 kcal/mol in enthalpy but unfavorable by 5.0 kcal/mol in free energy because of the entropy penalty. Two mechanisms (concerted metalation deprotonation CMD[24] and σ-bond metathesis[25]) are considered in the following C−H activation step.

DOI: 10.1021/acs.inorgchem.5b00134
Inorg. Chem. 2015, 54, 3958−3969

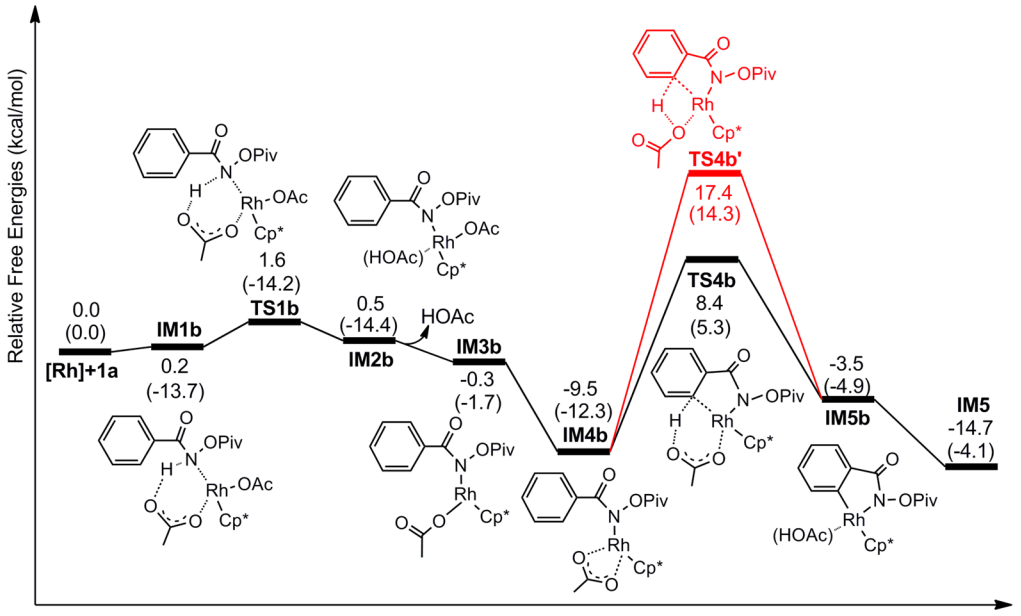

Figure 3. Free energy profile of Path B in the C−H activation step (values are given in kcal/mol; enthalpies are listed in parentheses).

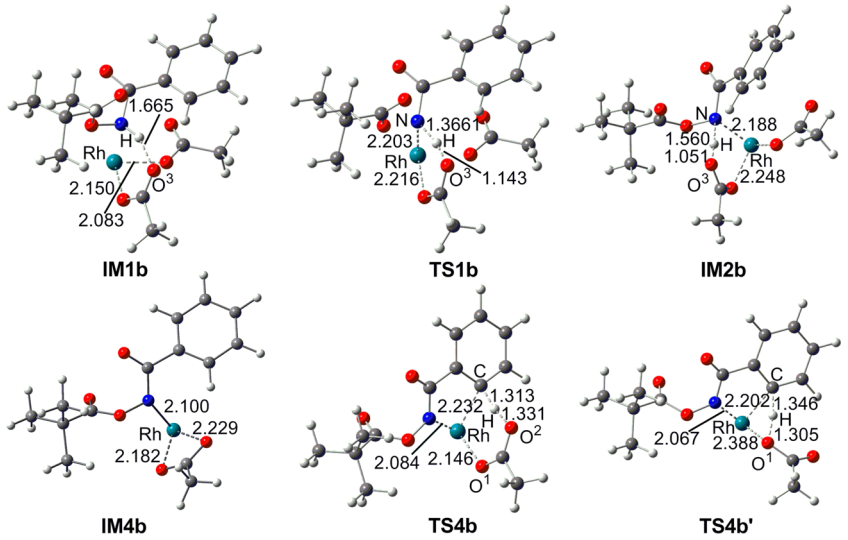

Figure 4. Optimized structures of the stationary points of Path B in the C−H activation step, along with the key bond lengths (in Angstroms). Cp* has been omitted for clarity.

In the CMD mechanism, activation of C−H bond is assisted by the C═O bond in OAc of [Rh] with the formation of a six-membered (Rh−C−H−O^2−C−O^1) transition state **TS1a** in which the distances of Rh−C, C−H, and H−O^2 are 2.302, 1.379, and 1.261 Å, respectively. Further weakening of C−H and Rh−O^1 and strengthening of Rh−C and H−O^2 give **IM2a** in which the distances of Rh−C, C−H, and H−O^2 are 2.066, 3.012, and 1.014 Å, indicating the cleavage of the C−H bond and the formation of Rh−phenyl. In the σ-bond metathesis mechanism, the transition state, **TS1a′**, features a distorted four-membered ring comprising of the Rh−O^1 and C−H bonds. The CMD mechanism is more favorable than σ-bond metathesis as the barrier of **TS1a′** (40.0 kcal/mol) is about 15 kcal/mol higher than that of **TS1a** (25.4 kcal/mol). Analyzing the geometries of **TS1a** and **TS1a′**, two reasons might be responsible for the high barrier of **TS1a′**: one is the larger distortion energy of four-membered ring in **TS1a′** than the six-membered one in **TS1a**; the other is that the stronger coordination between Rh and O^1 in **TS1a** increases the stability of **TS1a**. **IM3a** is produced with dissociation of HOAc from the Rh center of **IM2a**. Following **IM3a**, a hydrogen transfer transition state **TS3a** is located in gas phase with a barrier of 1.9 kcal/mol in electronic energy in which H transfers from N to O^3 atom. However, when considering the solvent effect, the energy of **TS3a** is 2.4 kcal/mol lower than **IM3a**, indicating that the hydrogen transfer is very facile in solvent. After the hydrogen transfer process, a new HOAc is formed in **IM4a** which is 2.6 kcal/mol more stable than **TS3a**. Once again, the HOAc is dissociated and five-membered rhodacycle intermediate **IM5** is formed with the bond lengths of Rh−N and Rh−C being 1.975 and 2.064 Å.

In Path B, N−H deprotonation is processed before C−H activation. As illustrated in Figure 3, **IM1b** is formed from the coordination of **1a** to the Rh center via the lone pair electrons of the N atom. Simultaneously, an extra hydrogen bond is formed in **IM1b** between N−H in **1a** and the O^3 atom in OAc. The interaction is slightly unfavorable by 0.2 kcal/mol in free energy

DOI: 10.1021/acs.inorgchem.5b00134
Inorg. Chem. 2015, 54, 3958−3969

Scheme 2. Four Coordination Modes Between 2a and IM5 and Corresponding Insertion Transition States

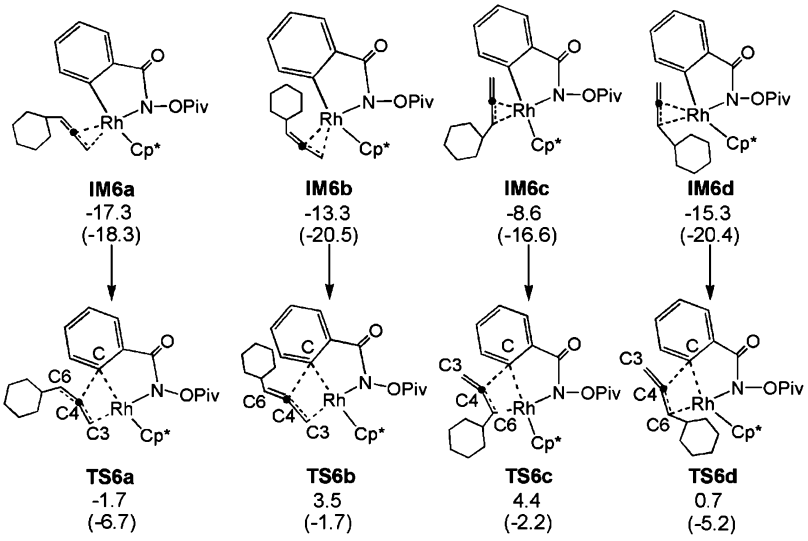

but more favorable by 13.7 kcal/mol in enthalpy, indicating **IM1b** is more easily generated than **IM1a**. Crossing a low barrier transition state **TS1b** (1.4 kcal/mol relative to **IM1b**) in which H transfers from N to the O^3 atom, **IM2b** is produced. In **IM2b**, the distances of Rh−N and H−O^3 further shorten to 2.188 and 1.051 Å and N−H lengthens to 1.560 Å, showing that a HOAc is formed. Release of HOAc gives **IM3b**. Isomerization of **IM3b** leads to **IM4b** and is exoergic by 9.2 kcal/mol. Following **IM4b**, two C−H activation mechanisms are considered as well (CMD and σ-bond metathesis). Similar to **TS1a**, in Path B, the CMD mechanism (**TS4b**, six-membered transition state with a barrier of 17.9 kcal/mol) is more favorable than a σ-bond metathesis mechanism (**TS4b′**, four-membered transition state about 26.9 kcal/mol). Through the C−H cleavage step, a new HOAc is formed in **IM5b**. Then **IM5** is generated after dissociation of HOAc.

From the discussion above, we can see that the CMD transition state is the rate-determining step both for Path A and for Path B. As far as two paths are concerned, the barrier of **TS1a** is 25.4 kcal/mol, which is much larger than that of **TS4b** (17.9 kcal/mol). This shows that Path B is a favorable pathway. In other words, the N−H deprotonation makes the following C−H activation much easier. Via N−H deprotonation, N coordinates to the Rh center which can increase the electron density of the Rh atom. The NBO charges of Rh for **IM4b** and **IM1a** are 0.430 and 0.500. Thus, the Rh atom in **IM4b** is more active for C−H activation. In addition, O^2 of acetate in catalyst provides a reaction site that makes the C−H activation feasible. Research about Rh(III)-catalyzed C−H functionalization with acetylene by Guimond et al. showed that the deprotonation of substrate is important for a low-barrier catalytic cycle.[22] Our present result is in agreement with their conclusion.

3.2. Carborhodation and Product Selectivity. There are four coordination modes between **2a** and **IM5** by different C═C double bonds coordinating with the Rh center as shown in Scheme 2. We calculated the structures of the intermediates and located the transition states for all coordination modes. **IM6a** is the most stable one. Carborhodations of allene give seven-membered cyclometalated Rh complexes via allene insertion transition states **TS6a**−**d**. The barriers of **TS6a**, **TS6b**, **TS6c**, and **TS6d** are −1.7, 3.5, 4.4, and 0.7 kcal/mol, respectively, relative to the original reactants. Therefore, the allene terminal C═C bond trans insertion into **IM5** is a favorable one.

In order to understand the regio- and stereoselectivity of the allenes insertion, a frontier molecular orbital [FMO] analysis was made for **IM5**, **2a**, **IM6a**−**d**, and **TS6a**−**d**.[26] As we know, the smaller the HOMO−LUMO energy gap is, the more reactive the reaction will be. Thus, the HOMOs and LUMOs energies of the **IM5** and **2a** were calculated. From Figure 5, we can see

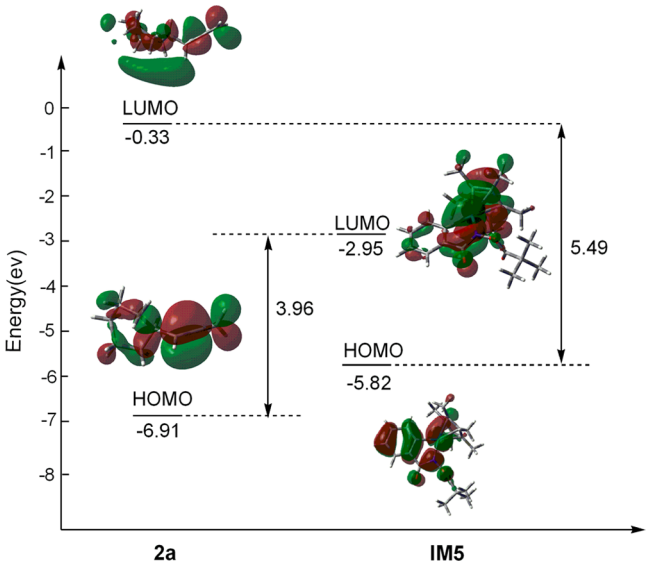

Figure 5. Energies of the HOMOs and LUMOs for **2a** and **IM5**.

that the E_{gap} of HOMO(**2a**)−LUMO(**IM5**) [3.96ev] is smaller than that of HOMO(**IM5**)−LUMO(**2a**) [5.49ev]. Therefore, the electrons transfer from the HOMO of **2a** in which the electrons mainly distribute at C3, C4, and C6 atoms to the LUMO of **IM5** in which the electrons mainly distribute at the Rh atom. Additionally, NBO analysis was performed in order to investigate the atom orbital contributions of C and Rh to the FMOs of **TS6a**−**d**. Table 1 lists the contributions of key atoms (Rh, C, C3/C6, and C4) to the HOMOs of **TS6a**−**d**, from which we can see that the total contributions of Rh, C, C3, and C4 atoms in **TS6a** are the largest among **TS6a**−**d**.

DOI: 10.1021/acs.inorgchem.5b00134
Inorg. Chem. 2015, 54, 3958−3969

Table 1. Contributions of Rh, C, C3/C6, and C4 Atoms to the HOMOs of TS6a−d

TS6a			TS6b			TS6c			TS6d		
Rh	d_{xy}	0.00%	Rh	d_{xy}	0.23%	Rh	d_{xy}	0.00%	Rh	d_{xy}	2.17%
	d_{xz}	0.10%		d_{xz}	2.35%		d_{xz}	1.20%		d_{xz}	0.08%
	d_{yz}	0.35%		d_{yz}	4.80%		d_{yz}	2.35%		d_{yz}	8.70%
	d_{x2y2}	1.45%		d_{x2y2}	2.24%		d_{x2y2}	6.19%		d_{x2y2}	5.48%
	d_{z2}	12.29%		d_{z2}	4.33%		d_{z2}	0.18%		d_{z2}	1.40%
C3	p_x	3.31%	C3	p_x	2.3%	C6	p_x	0.23%	C6	p_x	0.00%
	p_y	2.56%		p_y	2.89%		p_y	0.00%		p_y	5.24%
	p_z	0.26%		p_z	1.32%		p_z	7.50%		p_z	0.89%
C4	p_x	0.33%	C4	p_x	0.00%	C4	p_x	0.58%	C4	p_x	0.07%
	p_y	0.47%		p_y	2.64%		p_y	3.76%		p_y	0.19%
	p_z	4.24%		p_z	2.16%		p_z	0.19%		p_z	0.16%
C	p_x	2.48%	C	p_x	0.78%	C	p_x	0.53%	C	p_x	0.10%
	p_y	1.69%		p_y	0.03%		p_y	2.87%		p_y	0.36%
	p_z	1.67%		p_z	4.50%		p_z	2.13%		p_z	1.22%
		31.20%			30.57%			27.71%			26.06%

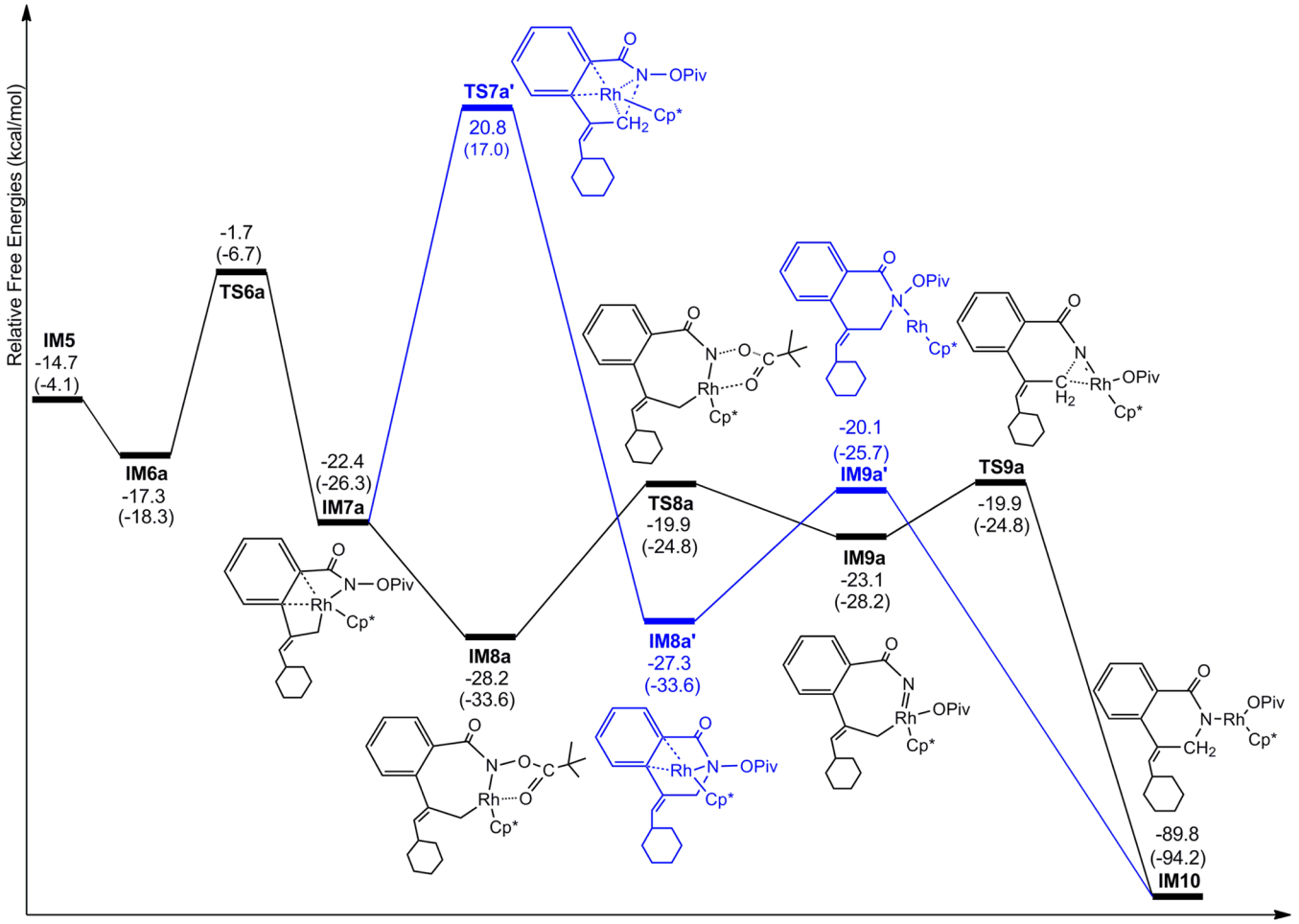

Figure 6. Free energy profile of the carborhodation step (values are given in kcal/mol; enthalpies are listed in parentheses).

This is consistent with our results that the barrier of **TS6a** is the lowest.

The mechanism of **IM6a** transformation is given in Figure 6, and the key structures are listed in Figure 7. In **TS6a**, the C^3═C^4 double bond inserts into the Rh−C bond. The distances of Rh−C, C−C^4, C^4−C^3, and C^3−Rh are changed from 2.154, 2.003, 1.421, and 2.105 Å in **TS6a** to 2.636, 1.503, 1.511, and 2.083 Å in **IM7a**, respectively. Two pathways are considered following **IM7a**. One is in the sequence of N−O cleavage and reductive elimination (black route in Figure 6); the other is in the reverse order (blue route in Figure 6). In the black pathway, **IM7a** first isomerizes to **IM8a** in which the C═O bond in the OPiv group turns to interact with the Rh center and is exoergic by 5.8 kcal/mol. Under the auxiliary interaction of C═O···Rh, the following N−O cleavage transition state (**TS8a**) is a five-membered ring with a low barrier of about 8.3 kcal/mol. The produced **IM9a** involves a Rh═N double bond. Reductive elimination of **IM9a** gives **IM10**. In the blue pathway, reductive

DOI: 10.1021/acs.inorgchem.5b00134
Inorg. Chem. 2015, 54, 3958−3969

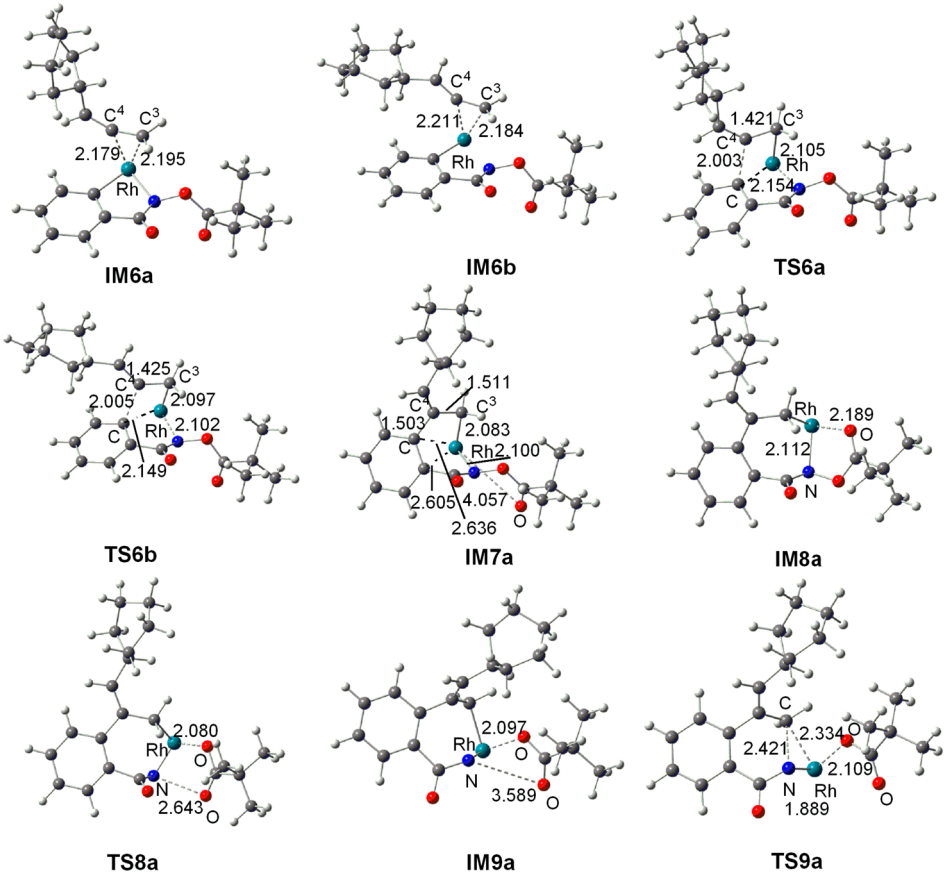

Figure 7. Optimized structures of the carborhodation step, along with the key bond lengths (in Angstroms). Cp* has been omitted for clarity.

elimination of **IM7a** is first processed through **TS7a′**. However, the barrier is considerably large, which is about 43.2 kcal/mol relative to **IM7a** and 20.8 kcal/mol to original reactants. Thus, the blue pathway can be ruled out.

In this step, the intermediate **IM8a** may rearrange to **IM9a″** through **TS8a″** with a barrier of 5.8 kcal/mol (Figure 8).

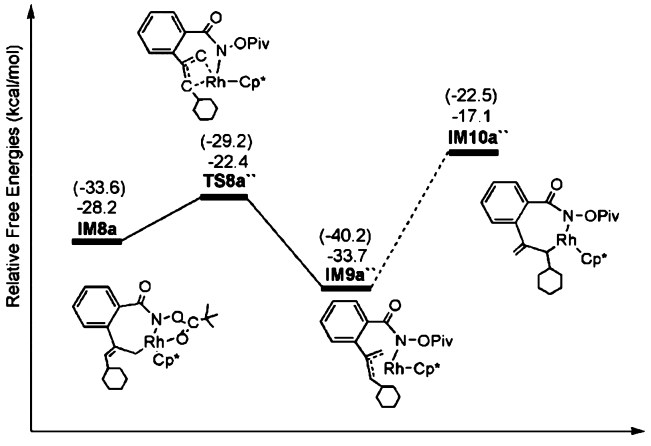

Figure 8. Free energy profile of the rearrangement of **IM8a** (values are given in kcal/mol; enthalpies are listed in parentheses).

This type of reaction can be found in many experimental and theoretical studies.[27] Then **IM9a″** transforms into **IM10a″** through the isomerization. Reductive elimination of **IM10a″** would lead to **3a″**. However, considering **IM10a″** is higher than **TS8a** and **TS9a** in free energy, the following reductive elimination of **IM10a″** should be more unfavorable, that is, **3a″** is impossible to be generated, which is consistent with the experiment.

3.3. Regeneration of Catalyst. To regenerate Cp*Rh-$(OAc)_2$ from **IM10**, two HOAc are necessary to substitute OPiv and **3a** moieties. According to the sequence of substitutions, two pathways are considered as listed in Figure 9. In the black pathway, through transition state **TS10a** (14.6 kcal/mol), **3a** is first generated from **IM10** with H of HOAc transferring to N and OAc transferring to Rh. Release of **3a** from **IM11a** gives **IM12a**. Then the second HOAc reacts with **IM12a** via six-membered metathesis transition state **TS12a** (11 kcal/mol relative to **IM12a**), giving HOPiv and Cp*Rh$(OAc)_2$. In the blue pathway, HOPiv is first released from **IM10** via **TS10a′**. **TS10a′** features an eight-membered ring with H of HOAc transferring to C═O in OPiv and C═O in HOAc interacting with Rh. Then **3a** and Cp*Rh$(OAc)_2$ are generated through metathesis between the second HOAc and **IM12a′** via **TS12a′**.

Analyzing the structure of **IM10**, we can see that if OPiv is not substituted by OAc it can act as OAc to process the N−H deprotonation, that is, **IM12a**, Cp*Rh(OAc)(OPiv), can catalyze the reaction as well. Thus, according to Path B in Figure 3, we calculated the N−H deprotonation and C−H activation of **1a** mediated by **IM12a**. Two pathways are considered, as both OPiv and OAc can accept the proton from **1a**. In the green path, OPiv accepts the proton and dissociates from Rh, giving **IM4b**, which can proceed to activate C−H with **TS4b** and lead to **IM5**. Then **IM5** will complete the following steps as we discussed in section 3.2. If OAc is a proton acceptor (black path in Figure 10), HOAc is first dissociated giving

DOI: 10.1021/acs.inorgchem.5b00134
Inorg. Chem. 2015, 54, 3958−3969

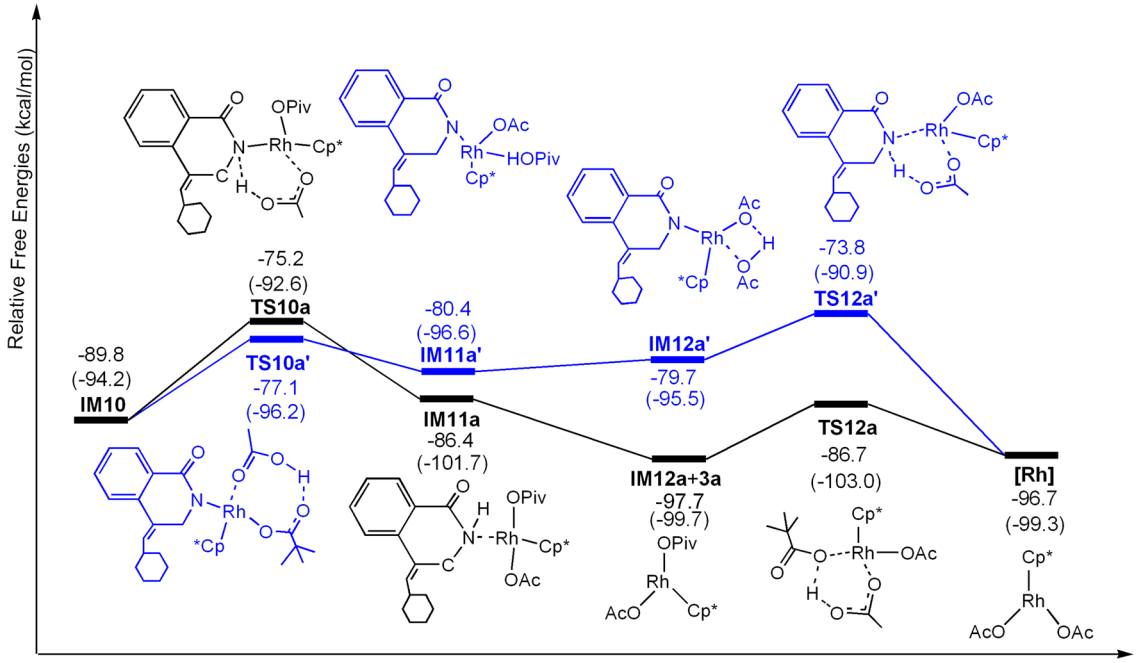

Figure 9. Free energy profile of regeneration of Cp*Rh(OAc)$_2$ (values are given in kcal/mol; enthalpies are listed in parentheses).

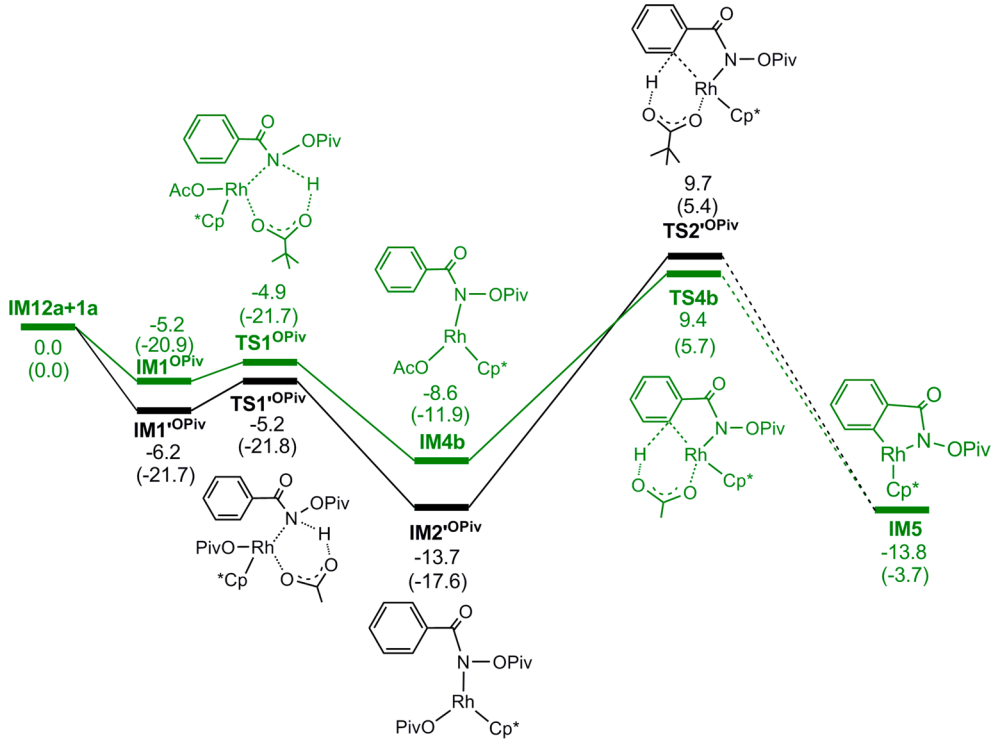

Figure 10. Free energy profile of N−H deprotonation and C−H activation mediated by Cp*Rh(OAc)(OPiv).

IM2′^{OPiv}. Crossing the C−H activation step (**TS2′^{OPiv}**), **IM5** resulted as well. The green path is slightly more favorable than the black one.

According to the calculated results, a barrier of 11 kcal/mol (**TS12a**) is needed for conversion of Cp*Rh(OAc)(OPiv) to Cp*Rh(OAc)$_2$. However, for both Cp*Rh(OAc)$_2$- and Cp*Rh(OAc)(OPiv)-catalyzed reactions, the rate-determining step, C−H activation (**IM4b−TS4b**), is about 18 kcal/mol, that is, in the first catalytic cycle, Cp*Rh(OAc)$_2$ is the catalyst. Nevertheless, once Cp*Rh(OAc)(OPiv) is generated, both Cp*Rh(OAc)$_2$ and Cp*Rh(OAc)(OPiv) can be catalyst.

3.4. Total Mechanism of 1a and 2a. Through detailed theoretical calculation, the mechanism of Rh(III)-catalyzed C−H activation and intermolecular annulation between **1a** and **2a** was understood. As discussed above, the whole reaction can be characterized by three steps, including (step I) C−H activation, (step II) carborhodation of allene, and (step III) regeneration of catalyst (Scheme 3). The product selectivity is decided by the carborhodation step.

DOI: 10.1021/acs.inorgchem.5b00134
Inorg. Chem. 2015, 54, 3958−3969

Scheme 3. Mechanism of Rh(III)-Catalyzed Reaction Between 1a and 2a

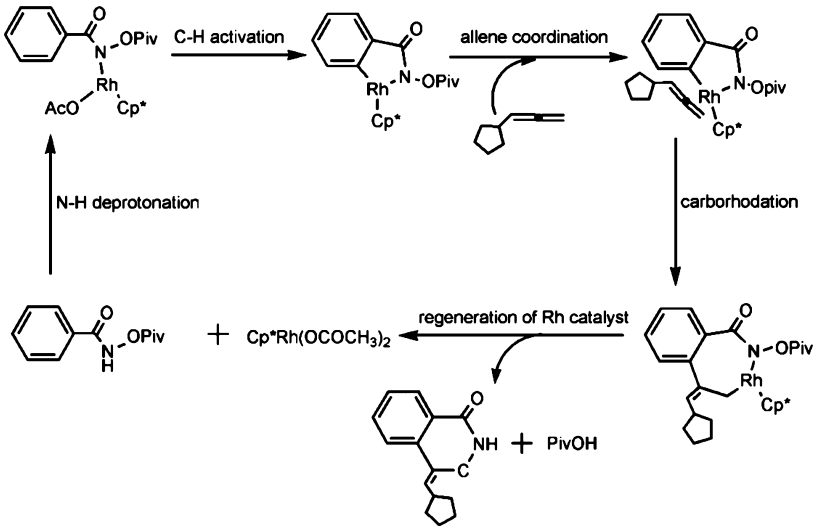

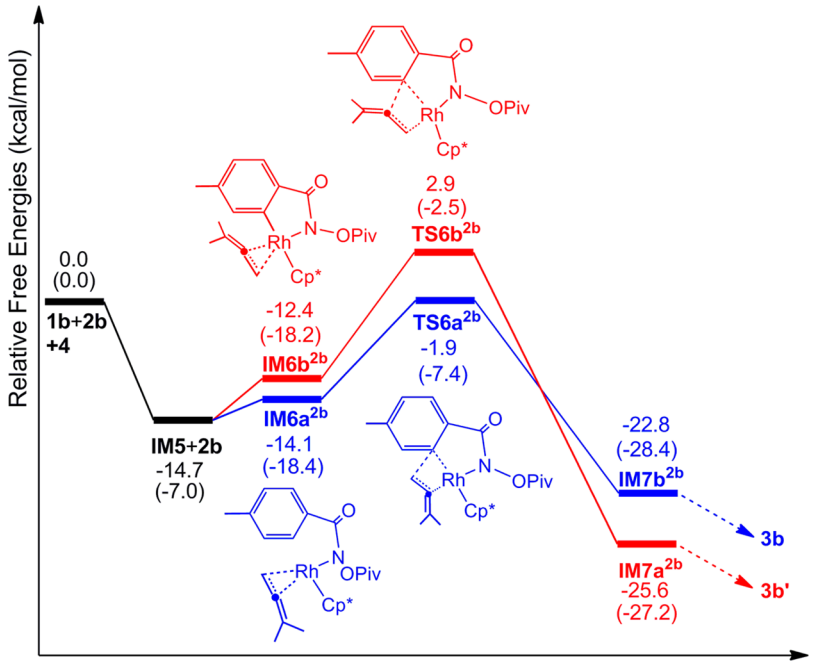

Figure 11. Free energy profile of the allene **2b** insertion step (values are given in kcal/mol; enthalpies are listed in parentheses).

3.5. Regioselectivity of the Reaction Between 1b and 2b. According to the mechanism of **1a** and **2a** discussed above, the regioselectivity lies in the carborhodation step. Thus, **2b** insertion into **IM5** is computed to figure out why only **3b** is produced. Two coordination modes can be employed between **2b** and **IM5**, **IM6a**,[2b] and **IM6b**,[2b] as shown in Figure 11. Through the insertion transition states (**TS6a**[2b] and **TS6b**[2b]), intermediates **IM7a**[2b] and **IM7b**[2b] are given which would be followed by reductive elimination, N−O cleavage, and regeneration of catalyst steps and eventually lead to **3b** and **3b′**. Both **IM6a**[2b] and **TS6a**[2b] are lower than the corresponding **IM6b**[2b] and **TS6b**,[2b] indicating **3b** is the favorable product which is consistent with the experiment. By analyzing the optimized structures (Figure 12), we can see that in **2b** insertion step, when allene is approaching Rh−C bond, the steric hindrance between the methyl and the benzyl group in **TS6b**[2b] is increased dramatically because the benzyl group in **TS6b**[2b] is rigid. However, in **TS6a**,[2b] methyl is approaching the flexible OPiv group, which can reduce the steric hindrance. Thus, the barrier of **TS6b**[2b] is higher than that of **TS6a**.[2b]

The FMO analysis is also employed for **IM5** and **2b**. The HOMOs and LUMOs energies of the **IM5** and **2b** are given in Figure 13. E_{gap} of HOMO(**2b**)−LUMO(**IM5**) [3.78ev] is smaller than that of HOMO(**IM5**)−LUMO(**2b**) [5.50ev]. Therefore, the electrons transfer from the HOMO of **2b** in which the electrons mainly distribute at the C3 and C4 atoms to the LUMO of **IM5** in which the electrons mainly distribute at the Rh atom. Table 2 lists the contributions of key atoms (Rh and C3/C4 atoms) to the HOMOs of **TS6a**[2b] and **TS6b**,[2b] from which we can see that the total contributions of Rh and C atoms in **TS6a**[2b] are much larger than **TS6b**.[2b] This is consistent with our results that the barrier of **TS6a**[2b] is lower.

3.6. Reaction Between 1c and 2a. The reaction mechanism of **1c** and **2a** with catalyst is computed to figure

DOI: 10.1021/acs.inorgchem.5b00134
Inorg. Chem. 2015, 54, 3958−3969

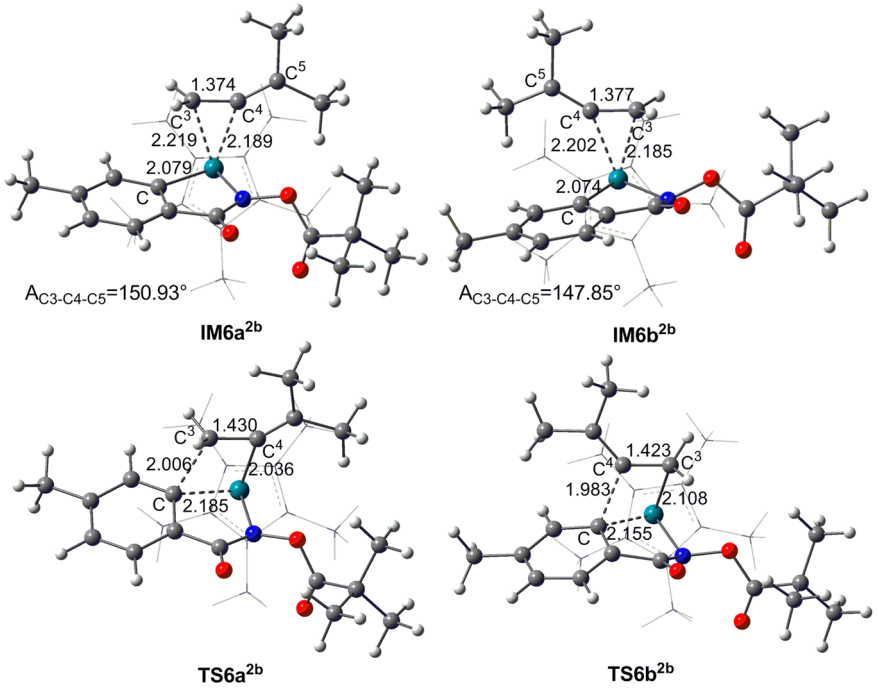

Figure 12. Optimized key structures in the **2b** insertion step, along with key bond lengths (in Angstroms).

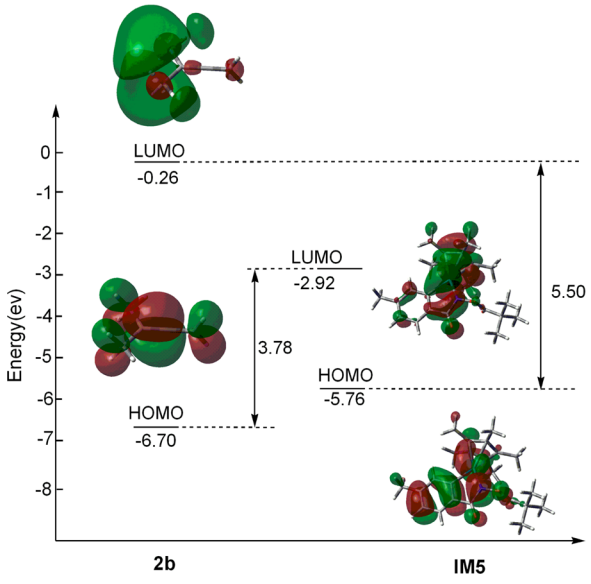

Figure 13. Energies of the HOMOs and LUMOs for **2b** and **IM5**.

Table 2. Contributions of Rh and C3/C4 Atoms to the HOMOs of TS6a^{2b} and TS6b^{2b}

TS6a^{2b}			TS6b^{2b}		
Rh	d_{yz}	10.18%	Rh	d_{xz}	3.85%
C4	p_z	3.79%	C3	p_z	2.38%
		13.97%			7.23%

out why no product is observed. Calculated results are demonstrated in Figure 14. From Figure 14, we can see that reaction between **1c** and **2a** is similar to that of **1a** and **2a**. Both processes experience N−H deprotonation (**TS1^{Me}**), C−H activation (**TS4^{Me}**), carborhodation (**TS6^{Me}**), N−O cleavage (**TS8^{Me}**), reductive elimination (**TS9^{Me}**), and finally regeneration of the catalyst. However, there is an obvious difference in N−O cleavage (**IM8^{Me}**−**TS8^{Me}** in Figure 15 and **IM8a**−**TS8a** in Figure 6). In **TS8a**, as discussed above, N−O cleavage is assisted by the C═O bond in OPiv with a five-membered transition state, while in **TS8^{Me}** no stabilization effect is provided. In **TS8^{Me}**, OMe transfers from N to Rh directly with a three-membered transition state and results in a large barrier of about 32.6 kcal/mol (relative to **IM8^{Me}**), which is higher than that of **TS8a** by 24.3 kcal/mol. Thus, **3a** could not be produced from **1c** and **2a**.

4. CONCLUSION

In summary, a detailed mechanism study on the mild Cp*Rh(OAc)$_2$-catalyzed C−H activation and intermolecular annulations between benzamide derivatives and allenes has been systematically conducted with DFT calculations. The study uncovers the origin of C−H activation and product selectivity for the reaction. The whole reaction involves three stages as (1) C−H activation induced by Rh catalyst interacting with benzamide derivatives, (2) allene carborhodation, and (3) regeneration of the catalyst. The results indicate that the N−H deprotonation first makes the C−H activation more facile. The reaction stereoselectivity depends on the type of C═C in allene coordinating into the Rh for reaction **1a** and **2a**. The trans insertion for the allene terminal C═C bond into Rh is the most favorable one. For reaction between **1b** and **2b**, the regioselectivity presented in carborhodation is controlled mainly by the steric hindrance effect. For reaction between **1c** and **2a**, the mechanism is similar to **1a** and **2a**. However, because the OPiv group is replaced by OMe, OMe transfers from N to Rh directly with a three-membered transition state which is much higher in energy than that of OPiv. Additionally, Cp*Rh(OAc)(OPiv) can be generated in a Cp*Rh(OAc)$_2$-catalyzed process. Once Cp*Rh(OAc)(OPiv) is produced, both Cp*Rh(OAc)$_2$ and Cp*Rh(OAc)(OPiv) can work as catalysts.

DOI: 10.1021/acs.inorgchem.5b00134
Inorg. Chem. 2015, 54, 3958−3969

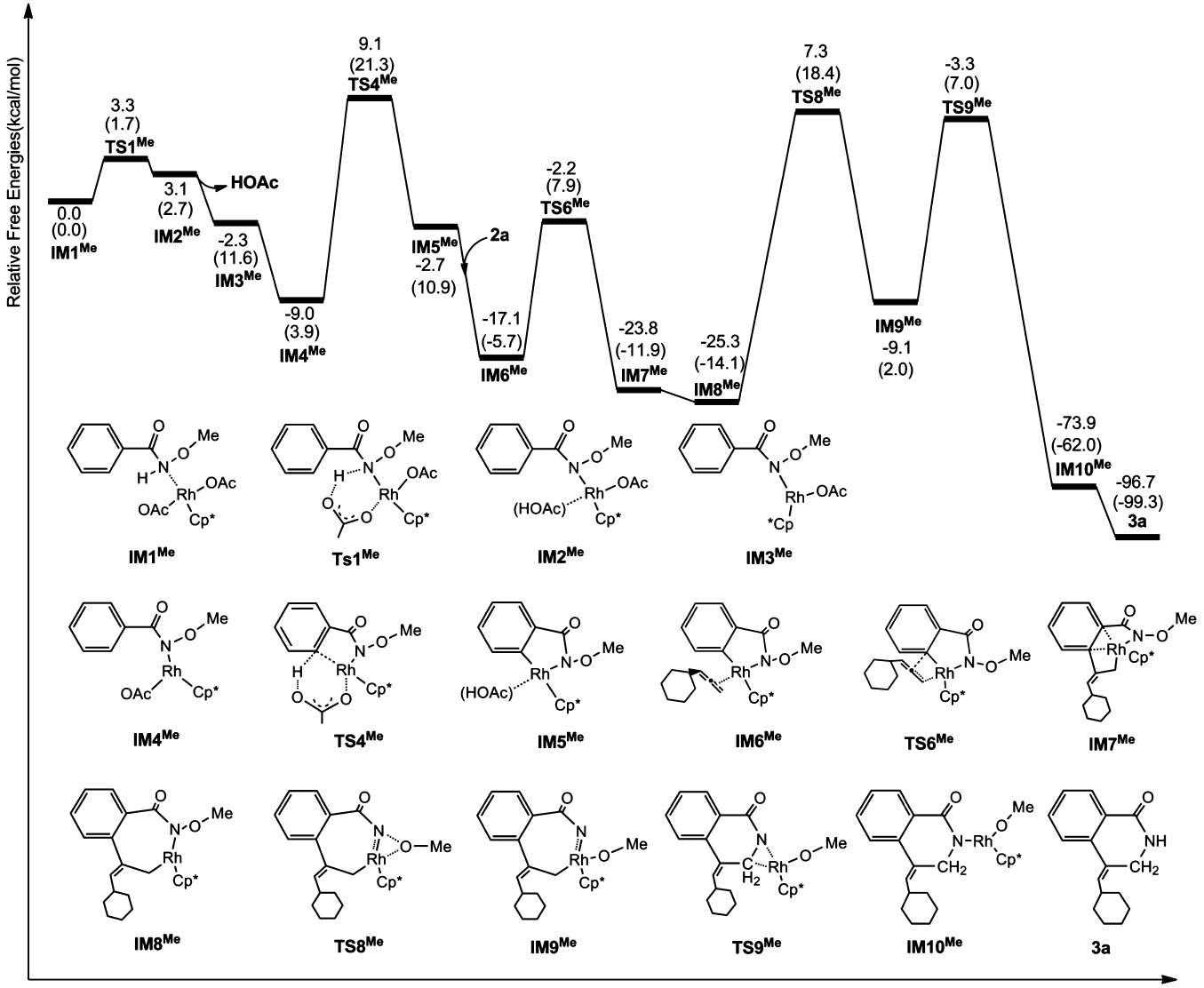

Figure 14. Free energy profile of the reaction between **1c** and **2a** (values are given in kcal/mol; enthalpies are listed in parentheses).

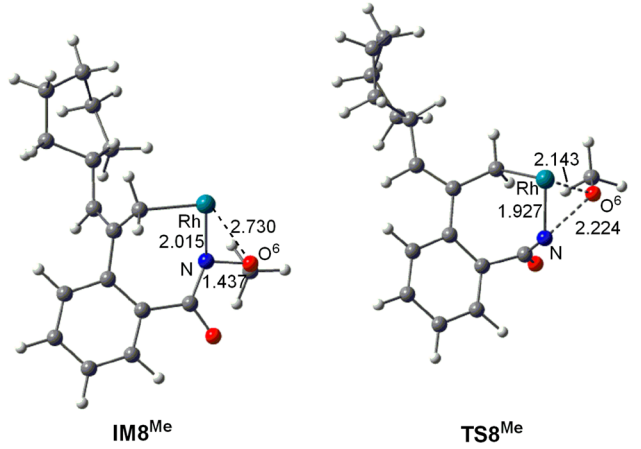

Figure 15. Optimized structures of **IM8**^{Me} and **TS8**^{Me}.

■ ASSOCIATED CONTENT

Supporting Information

Absolute enthalpies and Gibbs free energies and Cartesian coordinates of all structures involved in this study. This material is available free of charge via the Internet at http://pubs.acs.org.

■ AUTHOR INFORMATION

Corresponding Authors

*E-mail: huangf2004@163.com.

*E-mail: dchen@sdnu.edu.cn.

Notes

The authors declare no competing financial interest.

■ ACKNOWLEDGMENTS

This work was supported by the National Natural Science Foundations of China (Nos. 21375082, 21403132).

■ REFERENCES

(1) For selected reviews of metal-catalyzed cycloadditions see: (a) Lautens, M.; Klute, W.; Tam, W. *Chem. Rev.* **1996**, *96*, 49−92. (b) Yu, Z.-X.; Wang, Y. *Chem.—Asian J.* **2010**, *5*, 1072−1088. (c) Gulias, M.; Lopez, F.; Mascarenas, J. L. *Pure Appl. Chem.* **2011**, *83*, 495−506. (d) Lopez, F.; Mascarenas, J. L. *Beilstein J. Org. Chem.* **2011**, *7*, 1075−1094. (e) Neely, N.; Rovis, T. *J. Am. Chem. Soc.* **2013**, *135*, 66−69. (f) Seoane, A.; Casanova, N.; Quiñones, N.; Mascareñas, J. L.; Gulías, M. *J. Am. Chem. Soc.* **2013**, *136*, 834−837.

(2) For selected examples, see: (a) Stuart, D. R.; Bertrand-Laperle, M.; Burgess, K. M. N.; Fagnou, K. *J. Am. Chem. Soc.* **2008**, *130*, 16474−16475. (b) Shi, Z.; Zhang, C.; Li, S.; Pan, D.; Ding, S.; Cui, Y.; Jiao, N.

DOI: 10.1021/acs.inorgchem.5b00134
Inorg. Chem. 2015, 54, 3958−3969

Angew. Chem., Int. Ed. **2009**, *48*, 4572−4576. (c) Rakshit, S.; Patureau, F. W.; Glorius, F. *J. Am. Chem. Soc.* **2010**, *132*, 9585−9587. (d) Stuart, D. R.; Alsabeh, P.; Kuhn, M.; Fagnou, K. *J. Am. Chem. Soc.* **2010**, *132*, 18326−18339. (e) Huestis, M. P.; Chan, L.; Stuart, D. R.; Fagnou, K. *Angew. Chem., Int. Ed.* **2011**, *50*, 1338−1341. (f) Chen, J.; Pang, Q.; Sun, Y.; Li, X. *J. Org. Chem.* **2011**, *76*, 3523−3526.

(3) For selected examples, see: (a) Guimond, N.; Gouliaras, C.; Fagnou, K. *J. Am. Chem. Soc.* **2010**, *132*, 6908−6909. (b) Ackermann, L.; Lygin, A. V.; Hofmann, N. *Angew. Chem., Int. Ed.* **2011**, *50*, 6379−6382. (c) Dooley, J. D.; Reddy Chidipudi, S.; Lam, H. W. *J. Am. Chem. Soc.* **2013**, *135*, 10829−10836.

(4) (a) Larock, R. C.; Berrios-Peña, N. G.; Fried, C. A. *J. Org. Chem.* **1991**, *56*, 2615−2617. (b) Zeni, G.; Larock, R. C. *Chem. Rev.* **2006**, *106*, 4644−4680.

(5) (a) Yamauchi, M.; Morimoto, M.; Miura, T.; Murakami, M. *J. Am. Chem. Soc.* **2010**, *132*, 54−55. (b) Miura, T.; Yamauchi, M.; Kosaka, A.; Murakami, M. *Angew. Chem.* **2010**, *122*, 5075−5077. (c) Ochi, Y.; Kurahashi, T.; Matsubara, S. *Org. lett.* **2011**, *13*, 1374−1377.

(6) (a) Wang, H.; Beiring, B.; Yu, D.-G.; Collines, K. D.; Glorius, F. *Angew. Chem., Int. Ed.* **2013**, *52*, 12430−12434. (b) Huckins, J. R.; Bercot, E. A.; Thiel, O. R.; Hwang, T.-L.; Bio, M. M. *J. Am. Chem. Soc.* **2013**, *135*, 14492−14495. (c) Hyster, T. K.; Rovis, T. *J. Am. Chem. Soc.* **2010**, *132*, 10565−10569.

(7) (a) Kakiuchi, F.; Murai, S. *Acc. Chem. Res.* **2002**, *35*, 826−834. (b) Lyons, T. W.; Sanford, M. S. *Chem. Rev.* **2010**, *110*, 1147−1169. (c) Wencel-Delord, J.; Droge, T.; Liu, F.; Glorius, F. *Chem. Soc. Rev.* **2011**, *40*, 4740−4761.

(8) Wang, H.; Glorius, F. *Angew. Chem., Int. Ed.* **2012**, *51*, 7318−7322.

(9) Frisch, M. J.; Trucks, G. W.; Schlegel, H. B.; Scuseria, G. E.; Robb, M. A.; Cheeseman, J. R.; Scalmani, G.; Barone, V.; Mennucci, B.; Petersson, G. A.; Nakatsuji, H.; Caricato, M.; Li, X.; Hratchian, H. P.; Izmaylov, A. F.; Bloino, J.; Zheng, G.; Sonnenberg, J. L.; Hada, M.; Ehara, M.; Toyota, K.; Fukuda, R.; Hasegawa, J.; Ishida, M.; Nakajima, T.; Honda, Y.; Kitao, O.; Nakai, H.; Vreven, T.; Montgomery, J. A., Jr.; Peralta, J. E.; Ogliaro, F.; Bearpark, M.; Heyd, J. J.; Brothers, E.; Kudin,K. N.; Staroverov, V. N.; Kobayashi, R.; Normand, J.; Raghavachari, K.; Rendell, A.; Burant, J. C.;. Iyengar, S. S; Tomasi, J.; Cossi, M.; Rega, N.; Millam, J. M.; Klene, M.; Knox, J. E.; Cross, J. B.; Bakken, V.; Adamo, C.; Jaramillo, J.; Gomperts, R.; Stratmann, R. E.; Yazyev, O.; Austin, A. J.; Cammi, R.; Pomelli, C.; Ochterski, J. W.; Martin, R. L.; Morokuma, K.; Zakrzewski, V. G.; Voth, G. A.; Salvador, P.; Dannenberg, J. J.; Dapprich, S.; Daniels, A. D.; Farkas, Ö.; Foresman, J. B.; Ortiz, J. V.; Cioslowskiand, J.; Fox, D. J. *Gaussian 09*, Revision B.01; Gaussian, Inc.: Wallingford, CT, 2010.

(10) Lee, C.; Yang, W.; Parr, R. G. *Phys. Rev. B* **1988**, *37*, 785−789.

(11) (a) Beche, A. D. *J. Chem. Phys.* **1993**, *98*, 5648−5652. (b) Beche, A. D. *Phys. Rev. A: At. Mol. Opt. Phys.* **1988**, *38*, 3098−3100.

(12) (a) Hehre, W. J.; Ditchfield, R.; Pople, J. A. *J. Chem. Phys.* **1972**, *56*, 2257−2261. (b) Hariharan, P. C.; Pople, J. A. *Theor. Chim. Acta* **1973**, *28*, 213−222.

(13) (a) Hay, P. J.; Wadt, W. R. *J. Chem. Phys.* **1985**, *82*, 270−283. (b) Hay, P. J.; Wadt, W. R. *J. Chem. Phys.* **1985**, *82*, 299−310.

(14) Wadt, W. R.; Hay, P. J. *J. Chem. Phys.* **1985**, *82*, 284−298.

(15) Gonzalez, C.; Schlegel, H. B. *J. Phys. Chem.* **1990**, *94*, 5523−5527.

(16) Zhao, Y.; Truhlar, D. G. *Theor. Chem. Acc.* **2008**, *120*, 215−241.

(17) (a) Zhao, Y.; Truhlar, D. G. *Acc. Chem. Res.* **2008**, *41*, 157−167. (b) Kulkarni, A. D.; Truhlar, D. G. *J. Chem. Theory Comput.* **2011**, *7*, 2325−2332. (c) Zhao, Y.; Truhlar, D. G. *J. Chem. Theory Comput.* **2009**, *5*, 324−333.

(18) Marenich, A. V.; Cramer, C. J.; Truhlar, D. G. *J. Phys. Chem. B* **2009**, *113*, 6378−6396.

(19) (a) Green, A. G.; Liu, P.; Merlic, C. A.; Houk, K. N. *J. Am. Chem. Soc.* **2014**, *136*, 4575−4583. (b) Cheng, G.-J.; Yang, Y.-F.; Liu, P.; Chen, P.; Sun, T.-Y.; Li, G.; Zhang, X.; Houk, K. N.; Yu, J.-Q.; Wu, Y.-D. *J. Am. Chem. Soc.* **2014**, *136*, 894−897. (c) Hong, X.; Stevens, M. C.; Liu, P.; Wender, P. A.; Houk, K. N. *J. Am. Chem. Soc.* **2014**, *136*, 17273−17283. (d) Yang, Y.-F.; Cheng, G.-J.; Liu, P.; Leow, D.; Sun, T.-Y.; Chen, P.; Zhang, X.; Yu, J.-Q.; Wu, Y.-D.; Houk, K. N. *J. Am. Chem. Soc.* **2014**, *136*, 344−355.

(20) (a) Dang, Y.; Wang, Z.-X.; Wang, X. *Organometallics* **2012**, *31*, 7222−7234. (b) Dang, Y.; Wang, Z.-X.; Wang, X. *Organometallics* **2012**, *31*, 8654−8657. (c) Qu, S.; Dang, Y.; Wen, M.; Wang, Z.-X. *Chem.—Eur. J.* **2013**, *19*, 3827−3832. (d) Dang, Y.; Qu, S.; Wang, Z.-X.; Wang, X. *J. Am. Chem. Soc.* **2014**, *136*, 986−998.

(21) For recent reviews on Rh-catalyzed C-H bond activation, see: (a) Satoh, T.; Miura, M. *Chem.—Eur. J.* **2010**, *16*, 11212−11222. (b) Colby, D. A.; Bergman, R. G.; Ellman, J. A. *Chem. Rev.* **2010**, *110*, 624−655. (c) Colby, D. A.; Tsai, A. S.; Bergman, R. G.; Ellman, J. A. *Acc. Chem. Res.* **2012**, *45*, 814−825. (d) Neely, J. M.; Rovis, T. *J. Am. Chem. Soc.* **2013**, *135*, 66−69. (e) Patureau, F. W.; Wencel-Delord, J.; Glorius, F. *Aldrichimica Acta* **2012**, *45*, 31−41. (f) Kuhl, N.; Schröder, N.; Glorius, F. *Adv. Synth. Catal.* **2014**, *356*, 1443−1460.

(22) Guimond, N.; Gorelsky, S. I.; Fagou, K. *J. Am. Chem. Soc.* **2011**, *133*, 6449−6457.

(23) Xu, L.; Zhu, Q.; Huang, G.; Cheng, B.; Xia, Y. *J. Org. Chem.* **2012**, *77*, 3017−3024.

(24) (a) Gorelsky, S. I.; Lapointe, D.; Fagnou, K. *J. Org. Chem.* **2012**, *77*, 658−668. (b) Sokolov, V. I.; Troitskaya, L. L.; Reutov, O. A. *J. Org. Chem.* **1979**, *182*, 537−546. (c) Boutadla, Y.; Al-Duaij, O.; Davies, D. L.; Griffith, G. A.; Singh, K. *Organometallics* **2009**, *28*, 433−440. (d) Davies, D. L.; Donald, S. M. A.; Macgregor, S. A. *J. Am. Chem. Soc.* **2005**, *127*, 13754−13755. (e) García-Cuadrado, D.; de Mendoza, P.; Braga, A. A. C.; Maseras, F.; Echavarren, A. M. *J. Am. Chem. Soc.* **2007**, *129*, 6880−6886. (f) García-Cuadrado, D.; Braga, A. A. C.; Maseras, F.; Echavarren, A. M. *J. Am. Chem. Soc.* **2006**, *128*, 1066−1067.

(25) (a) Hennessy, E. J.; Buchwald, S. L. *J. Am. Chem. Soc.* **2003**, *125*, 12084−12085. (b) Mota, A. J.; Dedieu, A.; Bour, C.; Suffert, J. *J. Am. Chem. Soc.* **2005**, *127*, 7171−7182. (c) Gómez, M.; Granell, J.; Martinez, M. *Organometallics* **1997**, *16*, 2539−2546. (d) Gómez, M.; Granell, J.; Martinez, M. *J. Chem. Soc., Dalton Trans.* **1998**, 37−43.

(26) Hoffmann, R. *Rev. Mod. Phys.* **1988**, *60*, 601−628.

(27) (a) Ma, S. M. *Pure Appl. Chem.* **2006**, *72*, 197−208. (b) Yamanaka, M.; Kato, S.; Nakamura, E. *J. Am. Chem. Soc.* **2004**, *126*, 6287−6293. (c) Yoshikai, N.; Nakamura, E. *Chem. Rev.* **2011**, *112*, 2339−2372.

DOI: 10.1021/acs.inorgchem.5b00134
Inorg. Chem. 2015, 54, 3958−3969